



L. Wang · Y. J. Xie · H. Yuan

Potential fracture configurations of a cracked solid under mixed mode-I/III loading

Received: 3 July 2022 / Accepted: 29 January 2023 / Published online: 23 February 2023
© Springer-Verlag GmbH Germany, part of Springer Nature 2023

Abstract The potential fracture configurations of a cracked solid under mixed Mode-I/III loading are investigated based on a three-dimensional energy-based model, which can effectively capture the physical process of energy release induced by multiple cracks initiation from a crack tip. In order to maximize the energy release rate, four integral subintervals for J_i -integral around a crack tip have been suggested, based on which the four concerned energy-based driving forces have been identified. In this regard, when the driving forces reach the critical value, the concerned local boundaries around a crack tip will fracture, respectively, in a form of either wing cracks or crack extension. A series of potential fracture configurations for cracked solids under the mixed Mode-I/III loading, such as the crack tri-branching, symmetrical branching, side-branching, kinking and extension, can be theoretically predicted from the combination of the triggered new cracks. Some understanding on the fracture mechanism in engineering and experimental research should be refreshed based on the present theoretical investigations. Typical fracture configurations and concerned K-based effective fracture toughness predicted by the present modelling and Griffith's criterion agree well with the experimental results in the available literature.

Keywords Mode-I/III crack · Fracture configurations · Crack-branching

List of symbols

α_i, α_{ic}	Angle between the shifting direction of the local boundary and x_i -axis and its critical value
α	Inclined angle of the crack plane relative to the loading roller
r, θ	Polar coordinates
φ	Normalized parameter
μ	Poisson's ratio
σ_{ij}	Stress components
A, A_i, s, s_i	Boundary surfaces or integration paths around the crack tip
E	Young's modulus
G	Energy release rate for boundary shifting
$G^{\text{tri}-b}, G_{\text{max}}^{\text{tri}-b}, G_C^{\text{tri}-b}$	Energy release rate, its maximum and critical value for crack tri-branching

L. Wang · Y. J. Xie (✉) · H. Yuan
College of Petroleum and Natural Gas Engineering, Liaoning Petrochemical University, Fushun 113001, LN, People's Republic of China
e-mail: yjxiefs@qq.com

L. Wang
College of Pipeline and Civil Engineering, China University of Petroleum (East China), Qingdao 266000, SD, People's Republic of China

$G_{\max}^{\text{side-}b}, G_{\max}^{\text{sym-}b}, G_{\max}^{\text{kinking}}$	Energy-based configuration driving forces for crack side-branching, symmetrical-branching and kinking, respectively
$G_{\max}^{A\text{-ext}}$	Energy-based driving force for boundary A moving in x_1 -direction in a form of crack extension
$G_{\max}^{A\text{-wing}}$	Energy-based driving force for boundary A moving as a wing crack
J_i	Conservation integrals
$K_{\text{eff-}C}^{\text{tri-}b}, K_{\text{eff-}C}^{\text{side-}b}, K_{\text{eff-}C}^{\text{sym-}b}$	K-based effective fracture toughness for crack tri-branching, side-branching and symmetrical-branching, respectively
$K_{\text{eff-}C}^{A\text{-wing}}, K_{\text{eff-}C}^{A\text{-ext}}$	K-based effective fracture toughness for local boundary A moving as a wing crack or crack extension
K_{IC}	Fracture toughness for pure Mode-I crack extension
K_I, K_{III}	Stress intensity factors for the Mode-I or Mode-III deformations
P	Load
r_o	Polar coordinate of the boundary surface around crack tip
T_i	Stress vector acting on the integration surface or path
u_i	Displacement components
v_i	Direction of the local boundary A_i shifting
w	Strain energy density

1 Introduction

Fracture prediction depends on the fracture criterion [1]. However, the classical fracture theories, such as the maximum tangential stress criterion [2], the minimum strain energy density criterion [3] and the maximum energy release rate criterion [4], work well only for predicting a new born crack initiation from a crack tip. These well-known classical fracture theories cannot yet be used to predict some other potential fracture behaviours, such as the crack branching etc. Similar cases can be found in the other methods [5–11].

Planar crack propagation under pure Mode-I loading is generally stable and will become unstable with the superposition of a Mode-III loading [12, 13]. An initially flat parent crack segments into an array of daughter cracks that rotate towards a direction of maximum tensile stress [14]. Numerical simulations of mixed Mode-I/III brittle fracture using a continuum phase field method [15–17] indicated that planar crack propagation is linearly unstable against helical deformations of the crack front. During growth evolution, facets gradually coarsen in striking analogy with the coarsening of finger patterns observed in non-equilibrium growth phenomena. However, the crack initiation behaviour and its mechanism for a well-defined mixed Mode-I/III crack are still foundational issues which govern the subsequent potential evolution of the crack surface.

Fracture criterion should have predicted various potential fracture behaviours, such as the crack propagation and branching. As the crack branching can be observed not only at the Mode-I crack tip, but also at the Mode-II and mixed Mode-I/II crack tips, it is therefore reasonable to speculate that the similar fracture behaviour should happen at the mixed Mode-I/III crack tip. Usually, if a crack tip split into two or more crack tips, the stress intensity factors for the newborn cracks are smaller in varying degrees than that for the original crack [18], which may change the crack growth behaviours. The fracture mechanism also plays a major role in the engineering applications, such as the formation of the hydraulic crack system during hydraulic fracturing. A good understanding on crack propagation, branching conditions and mechanism is important to explain and predict the complex fracture phenomenon.

Recently, a two-dimensional energy-based modelling had been suggested to simulate the physics process involved in multiple cracks initiation from a crack tip under Mode-I, Mode-II and mixed Mode-I/II loading [19–23]. In present article, this modelling has been extended to three-dimensional one and used to formulize the multiple cracks initiation from a crack tip under mixed Mode-I/III loading. Some potential fracture configurations, including the mixed Mode I/III crack tri-branching, symmetrical-branching, side-branching, kinking and extension, are investigated in detail. The possible crack initiation angles, the associated energy-based configuration driving forces and the K-based effective fracture toughness are found within the framework of the linear elastic fracture mechanics.

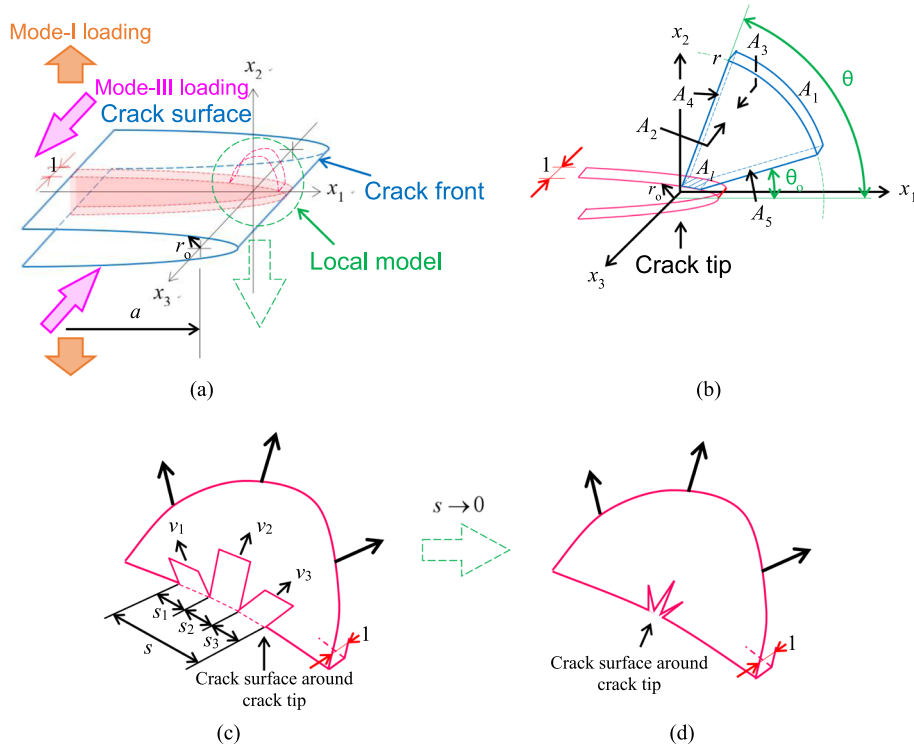


Fig. 1 Geometrical modelling of multiple cracks initiation from a crack tip (in case of $m = 3$) when $s \rightarrow 0$. **a** A cracked solid under mixed Mode-I/III loading ($r_0 \rightarrow 0^+$). **b** Typical local integral surfaces within the K-dominant region. **c** Multiple-notches model for boundaries A_i ($i = 1, 2, 3$) shifting. **d** Model for multiple cracks initiation

2 Three-dimensional geometrical and fracture modelling

Figure 1 shows a cracked solid subjected to mixed Mode-I/III loading. The x_3 -axis is along the crack front, and x_2 is normal to the crack surface. A plate-shaped segment, bounded by two planes paralleling to the x_1 - x_2 plane at unit distance from each other and a longitudinal closed surface, can be detached from the cracked solid as shown in Fig. 1a, c and d, which will be used as a three-dimensional modelling to formulized the physical process of energy release for potential multiple cracks initiation from the local boundary around crack tip.

Multiple cracks initiation from a boundary within the K-dominant region can be geometrically considered as multiple boundaries shifting in different directions as shown in Fig. 1c. When the local crack surfaces $A_i = s_i \times 1$ shift in v_i -direction ($i = 1, 2, 3, \dots, m$), m notches should be formed and will degenerate into m cracks with the width $s = s_1 + s_2 + \dots + s_m \rightarrow 0$ as shown in Fig. 1d in the case of $m = 3$. Then, from the local boundary surface $A = A_1 + A_2 + \dots + A_m \rightarrow 0$, a three-dimensional geometrical modelling for multiple cracks initiation in m directions can be proposed and sketched in Fig. 1d. This modelling is actually the three-dimensional extension from the two-dimensional one [19–24]. For the geometrical configuration of boundary shifting as shown in Fig. 1c, d, the energy release rate can be given by [19–24]

$$G = \lim_{A \rightarrow 0} \iint_A w e_i n_i d\Omega = \sum_{l=1}^m \left(\lim_{s_l \rightarrow 0} \iint_{A_l} w e_i n_i d\Omega \right), \quad (1)$$

where $e_i = \cos \alpha_i$ and α_i is the angle between shifting direction v_l of the boundary A_l and x_i -axis illustrated in Fig. 1c; n_i is the unit normal vector of the boundary A_l . By using the three-dimensional conservation law [24, 25], Eq. (1) may be expressed by

$$G = \sum_{l=1}^m \{ J_1(A_l)|_{A_l \rightarrow 0} \cos(\alpha_1)_l + J_2(A_l)|_{A_l \rightarrow 0} \cos(\alpha_2)_l + J_3(A_l)|_{A_l \rightarrow 0} \cos(\alpha_3)_l \}, \quad (2)$$

where

$$J_j(A_l)|_{A_l \rightarrow 0} = \lim_{A_l \rightarrow 0} \iint_{A_l} wn_j d\Omega = \iint_{(A_{in})_l} (wn_j - T_i u_{i,j}) d\Omega, \quad j = 1, 2, 3 \tag{3}$$

and $(A_{in})_l, (l = 1, 2, \dots, m)$, is an integral surface within the solids; $(A_{in})_l - A_l$ becomes a closed one. The $J_j(A_l)|_{A_l \rightarrow 0}$ in Eq. (3) is the energy release rate when the boundary A_l shifts in x_j -direction.

Unlike the applications of the classical fracture criterion, when Eq. (2) is applied to formulize the multiple cracks initiation, the integral subintervals for J_j -integrals should be determined first. Then, the maximized energy release rate for multiple cracks initiation can be found based on the positive/negative features of $J_j(A_l)|_{A_l \rightarrow 0}$ -integrals. It should be indicated that when the local boundary surface A_l moves inward to solids, $J_j(A_l)|_{A_l \rightarrow 0}$ may be positive or negative. If $J_j(A_l)|_{A_l \rightarrow 0} > 0.0$, the cracking induced by A_l moving inward to solids will lead strain energy release, which may occur naturally. If $J_j(A_l)|_{A_l \rightarrow 0} < 0.0$, the so-called cracking should lead to energy absorbing, which is impossible to happen naturally. Then, Eq. (2) must include all the contributions of the positive energy release for the $A_l, (l = 1, 2, \dots, m)$, shifting inward to solids in order to maximize the energy release rate. The negative $J_j(A_l)|_{A_l \rightarrow 0}$ should be excluded from Eq. (2), because which violates the principle of energy release [12–16]. In this case, the maximized energy release rate becomes a real energy-based configuration driving force, which exhibits a fracture modelling to capture the physical process of multiple cracks initiation.

3 Positive/negative features on J_j -integrals

The positive/negative features of the J_j -integrals can be easily revealed by analysing its integrands, based on which the number m of the subintervals can be found.

3.1 J_j -integrals

A well-defined crack tip can be enlarged as a U-turn-shaped crack surface with unit width and $r_o \rightarrow 0^+$ as shown in Fig. 1b. When $(A_{in})_l = \sum_{i=1}^5 A_i$, where A_1 is a cylindrical surface within the K-dominant region, from Eq. (3), the J_j -integrals over A_l can be given by

$$J_j(A_l)|_{A_l \rightarrow 0} = \lim_{A_l \rightarrow 0} \iint_{A_l} wn_j d\Omega = \iint_{\sum_{i=1}^5 A_i} (wn_j - T_i u_{i,j}) d\Omega \stackrel{r \rightarrow r_o}{=} \iint_{A_1} (wn_j - T_i u_{i,j}) d\Omega, \quad j = 1, 2, \text{ and } 3. \tag{4}$$

For any local crack surface $A_l = \{A | r_o \rightarrow 0^+, \theta \in [\theta_0, \theta], x_3 \in [-0.5, 0.5]\}$ as shown in Fig. 1b, substituting the stress and displacement within the K-dominant region into Eq. (4), the J_j -integrals over the surface A_l can be found, respectively, as

$$J_1(A_l) = \frac{1 - \mu^2}{2\pi E} \int_{\theta_0}^{\theta} \left[K_I^2 (1 - \cos 2\theta) + \frac{1}{1 - \mu} K_{III}^2 \right] d\theta, \tag{5}$$

$$J_2(A_l) = \frac{1 - \mu^2}{2\pi E} \int_{\theta_0}^{\theta} (-K_I^2 \sin 2\theta) d\theta \tag{6}$$

and

$$J_3(A_l) = 0. \tag{7}$$

It should be noted that as $J_3(A_l) = 0$, the newborn crack surface or crack tip does not move in x_3 -direction, which means that the new crack tip still remains in the x_1 - x_2 plane. Additionally, Eq. (6) does not contain any contribution of K_{III} , which implies that the behaviours of $J_2(A_l)$ -integral are similar to the case of pure Mode-I deformation [22].

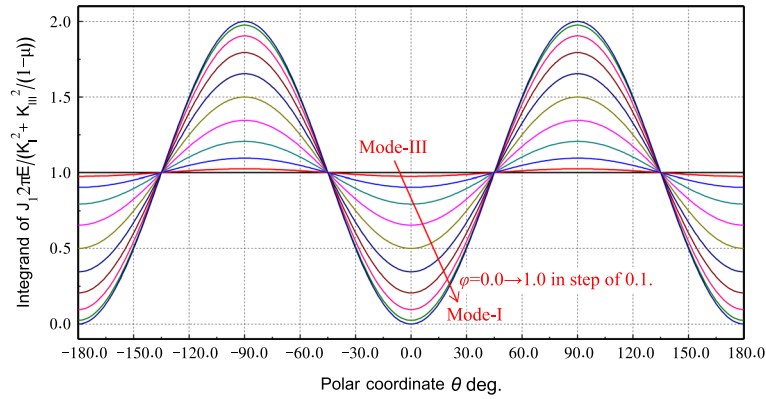


Fig. 2 Integrand of normalized J_1 -integral

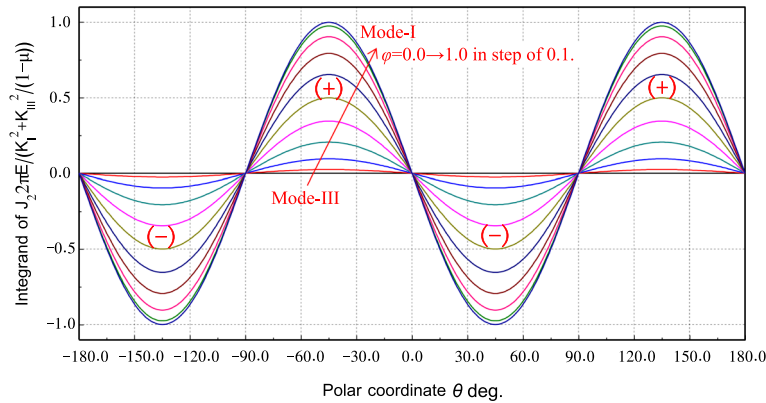


Fig. 3 Integrand of normalized J_2 -integral

For convenience of subsequent analysis, introduce a normalized parameter

$$\varphi = \frac{2}{\pi} \arctan \frac{K_I}{K_{III}/\sqrt{1-\mu}}, \tag{8}$$

which varies from 0.0 for pure Mode-III deformation to 1.0 for pure Mode-I and may completely describe the relative strength of K_I and K_{III} . By using Eq. (8), Eqs. (5) and (6) become

$$J_1(A_I) = \frac{(1-\mu^2)(K_I^2 + K_{III}^2/(1-\mu))}{2\pi E} \int_{\theta_0}^{\theta} \left(1 - \sin^2 \frac{\pi\varphi}{2} \cos 2\theta\right) d\theta \tag{9}$$

and

$$J_2(A_I) = \frac{(1-\mu^2)(K_I^2 + K_{III}^2/(1-\mu))}{2\pi E} \int_{\theta_0}^{\theta} -\sin^2 \frac{\pi\varphi}{2} \sin 2\theta d\theta. \tag{10}$$

Equation (9) shows that the integrand of the normalized $J_1(A_I)$ -integral always takes on positive value, i.e. $1 - \sin^2(\pi\varphi/2) \cos 2\theta \geq 0$ on $-\pi \leq \theta \leq \pi$ as illustrated in Fig. 2, which means the energy release when any local boundary A_I shifts in x_1 -direction. Unlike Eq. (9), Eq. (10) shows that the integrand of the normalized $J_2(A_I)$ -integral may take on both positive and negative values as shown in Fig. 3.

3.2 J_2 -integral

For a cracked solid under mixed Mode-I/III loading, five intersection points of the integrand of normalized J_2 -integral and θ -axis can be found by setting $\sin^2(\pi\varphi/2) \sin 2\theta = 0$, i.e.

$$\theta_k = \frac{k\pi}{2}, k = 0, \pm 1, \pm 2. \tag{11}$$

Table 1 Normalized $J_j(A_l)$ -integrals

Normalized $J_j(A_l)$ -integrals	$A_1 = \{A r = r_o, \theta \in [0, \pi/2], x_3 \in [-0.5, 0.5]\}$ $A_3 = \{A r = r_o, \theta \in [-\pi, -\pi/2], x_3 \in [-0.5, 0.5]\}$	$A_2 = \{A r = r_o, \theta \in [\pi/2, \pi], x_3 \in [-0.5, 0.5]\}$ $A_4 = \{A r = r_o, \theta \in [-\pi/2, 0], x_3 \in [-0.5, 0.5]\}$
$2\pi EJ_1(A_l)/(1-\mu^2)$	$\pi/2$	$\pi/2$
$(K_I^2 + K_{III}^2)/(1-\mu)$	$-\sin^2(\pi\varphi/2)$	$\sin^2(\pi\varphi/2)$
$2\pi EJ_2(A_l)/(1-\mu^2)$		
$(K_I^2 + K_{III}^2)/(1-\mu)$		

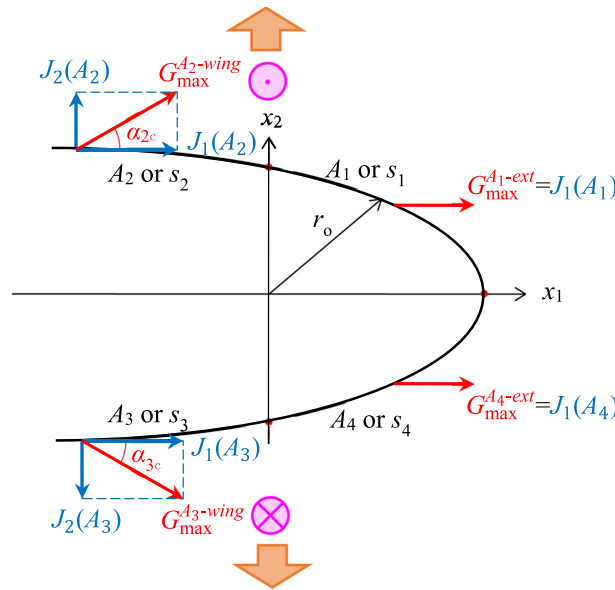


Fig. 4 Division of subintervals, energy-based driving forces and the fracture trends. ($r_o \rightarrow 0^+$)

As sketched in Fig. 3, these intersection points should divide the interval $[\pi, -\pi]$ into four subintervals, i.e. $[0, \pi/2]$ and $[\pi/2, \pi]$ for the upper crack surface, $[-\pi, -\pi/2]$ and $[-\pi/2, 0]$ for the lower crack surface, which is similar to the case of the pure Mode-I deformation [20, 22]. Figure 3 indicates that the integrand of the normalized $J_2(A_l)$ -integral $-\sin^2(\pi\varphi/2) \sin 2\theta \leq 0$ on $[0, \pi/2]$ and $[-\pi, -\pi/2]$; $-\sin^2(\pi\varphi/2) \sin 2\theta \geq 0$ on $[\pi/2, \pi]$ and $[-\pi/2, 0]$. The $J_2(A_l)$ -integral over the four subintervals takes on either positive or negative value and is summarized in Table 1.

The physical meanings of the positive and negative J_2 -integrals are different, which determine the division of the integral subintervals and the distribution of energy-based driving forces. For the upper half a crack tip boundary, $A_1 = \{A|r_o, \theta \in [0, \pi/2], x_3 \in [-0.5, 0.5]\}$ and $A_2 = \{A|r_o, \theta \in [\pi/2, \pi], x_3 \in [-0.5, 0.5]\}$, $J_2(A_1) < 0$ and $J_2(A_2) > 0$ theoretically indicate that if the boundary A_1 moves in x_2 -direction, the cracked solids will absorb or increase strain energy, which actually is impossible to occur naturally; if the A_2 moves in the x_2 -direction, the solid will release the energy. So, viewed from maximizing energy release rate, the contribution of $J_2(A_1)$ should be excluded from Eq. (2) with the aid of the reasonable division of subintervals. For the boundaries $A_3 = \{A|r = r_o, \theta \in [-\pi, -\pi/2], x_3 \in [-0.5, 0.5]\}$ and $A_4 = \{A|r = r_o, \theta \in [-\pi/2, 0], x_3 \in [-0.5, 0.5]\}$ for the lower half a crack tip surface, when A_3 moves in the opposite x_2 -direction, the energy release rate $-J_2(A_3) > 0$, which means that a crack initiation from A_3 as a wing crack is possible; when A_4 moves in the opposite x_2 -direction, $-J_2(A_4) < 0$ implies that this form of boundary moving will cause energy-absorbing and is not going to happen. The potential energy-based driving forces acting, respectively, on A_1, A_2, A_3 and A_4 and the potential crack initiation angles are shown in Fig. 4. It should be noted that the energy-based driving force has three basic elements, such as the point of application, direction and magnitude.

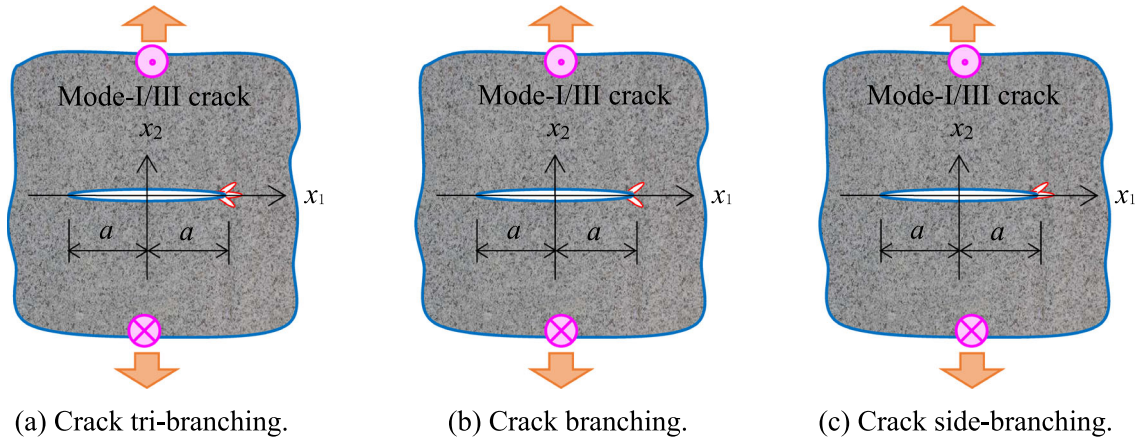


Fig. 5 Basic fracture configurations for multiple cracks initiation

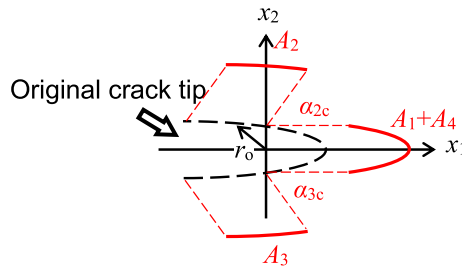


Fig. 6 The geometrical sketch on three cracks initiation from a Mode-I/III crack tip

The analysis of this section implies that the subinterval number m should be no larger than 4.

4 Multiple-cracks initiation from a mixed Mode-I/III crack tip

The above analysis implies that when the energy-based driving forces acting, respectively, on the four subintervals reach the critical value, the concerned local boundaries around a crack tip will fracture. Any real fracture configuration is one of the potential fracture configurations, which may be a triggered new born crack or the combination of multiple new born cracks under proper conditions.

For a mixed Mode-I/III crack, there are five basic potential fracture configurations, i.e. the crack tri-branching (-shaped fracture), branching (-shaped symmetrical fracture), side-branching (-shaped fracture) as shown in Fig. 5, kinking and extension. The detailed analysis will be given in this section.

4.1 Configuration driving force and fracture angles for mixed Mode-I/III crack tri-branching

Based on the discussions in Sect. 3.2, the fracture configuration of crack tri-branching may be created when boundaries A_2 and A_3 move inward to solid as two wing cracks and $A_1 + A_4$ moves together in x_1 -direction in form of the original crack extension as illustrated in Figs. 4, 5a and 6. In this regard, the whole boundary around crack tip is actually divided to three subboundaries ($m = 3$), i.e. A_2 , A_3 and $A_1 + A_4$, on which there are three energy-based driving forces acting, respectively, as shown in Fig. 4. By using the symmetry of the tri-fractures configuration, the concerned energy release rate can be given by

$$G^{\text{tri-b}} = 2(J_1(A_1) \cos \alpha_1 + J_1(A_2) \cos \alpha_2 + J_2(A_2) \sin \alpha_2) \tag{12}$$

from Eq. (2). By substituting the results in Table 1 into Eq. (12), the following expression can be found.

$$G^{\text{tri-b}} = \frac{(1 - \mu^2)(K_I^2 + K_{III}^2/(1 - \mu))}{2E} \left\{ \cos \alpha_1 + \sqrt{1 + (4/\pi^2) \sin^4(\pi\varphi/2) \cos(\alpha_2 - \beta)} \right\}, \tag{13}$$

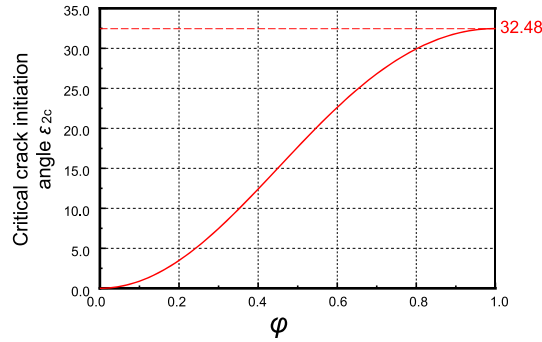


Fig. 7 Critical crack initiation angle α_{2c}

where

$$\beta = \tan^{-1}[(2/\pi) \sin^2(\pi\varphi/2)] \text{ deg.} \tag{14}$$

To find the maximised energy release rate, we set $\frac{\partial G^{\text{tri-b}}}{\partial \alpha_i} = 0$, $i = 1$ and 2 , and obtain $\sin \alpha_{1c} = 0$ and $\sin(\alpha_{2c} - \beta) = 0$, which give

$$\alpha_{1c} = \alpha_{4c} = 0 \text{ deg.} \tag{15}$$

and

$$\alpha_{2c} = -\alpha_{3c} = \beta \text{ deg.,} \tag{16}$$

where α_{1c} and α_{2c} , schematically shown in Figs. 4 and 7, are the theoretical expected critical crack initiation angles at which $G^{\text{tri-b}}$ reaches its maximum value and can be given by

$$G_{\text{max}}^{\text{tri-b}} = \frac{(1 - \mu^2)(K_I^2 + K_{III}^2/(1 - \mu))}{E} \frac{1 + \sqrt{1 + (4/\pi^2) \sin^4(\pi\varphi/2)}}{2}. \tag{17}$$

Equation (17) denotes an energy-based configuration driving force for mixed Mode-I/III crack tri-branching as shown in Figs. 5a and 6. It indicates that when

$$G_{\text{max}}^{\text{tri-b}} = G_C^{\text{tri-b}}, \tag{18}$$

the mixed Mode-I/III crack will theoretically fracture in the form of crack tri-branching.

4.2 K-based effective fracture toughness for Mode-I/III crack tri-branching

For the cracked brittle solids, the Griffith's criterion [26] states that a crack will initiate when the driving force or applied G_{max} reaches its critical value G_C [26, 27], i.e.

$$G_{\text{max}} = G_C. \tag{19}$$

For pure Mode-I deformation, when $G_{\text{max}} = G_C$, we have

$$G_C = \frac{(1 - \mu^2)K_{IC}^2}{E}. \tag{20}$$

When the mixed Mode-I/III crack tri-branching is triggered, as discussed in Sect. 4.1, the energy-based driving force acting on A_2 or A_3 can be found as

$$G_{\text{max}}^{A_2\text{-wing}} = \frac{(1 - \mu^2)(K_I^2 + K_{III}^2/(1 - \mu))}{E} \frac{\sqrt{1 + (4/\pi^2) \sin^4(\pi\varphi/2)}}{4}. \tag{21}$$

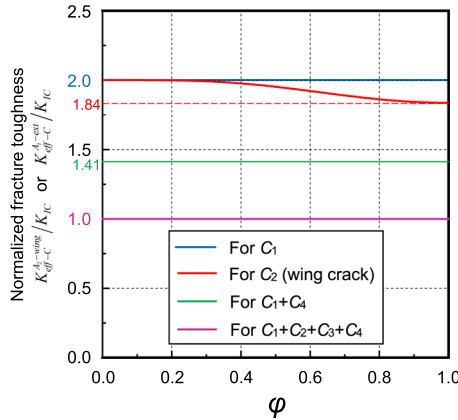


Fig. 8 Normalized fracture toughness $K_{\text{eff}-C}^{A_2\text{-wing}} / K_{IC}$ and $K_{\text{eff}-C}^{A_1\text{-ext}} / K_{IC}$ for local boundaries

The energy-based driving force triggering $A_1 + A_4$ to fracture as a form of crack extension can be expressed by

$$G_{\text{max}}^{A_1+A_4\text{-ext}} = \frac{(1 - \mu^2)(K_I^2 + K_{III}^2/(1 - \mu))}{E} \frac{1}{2}. \tag{22}$$

From Eqs. (19)-(22), it is not difficult to find the K-based fracture toughness

$$K_{\text{eff}-C}^{A_2\text{-wing}} = \frac{2}{[1 + (4/\pi^2) \sin^4(\pi\phi/2)]^{1/4}} K_{IC} \tag{23}$$

for wing crack, where the effective stress intensity factor $K_{\text{eff}} = \sqrt{K_I^2 + K_{III}^2/(1 - \mu)}$, and

$$K_{\text{eff}-C}^{A_1+A_4\text{-ext}} = 1.41 K_{IC} \tag{24}$$

for main crack extension as shown in Fig. 8. Then, from Eqs.(17) and (18), the critical energy release rate for crack tri-branching can be found as

$$G_C^{\text{tri}-b} = \frac{(1 - \mu^2)(K_{\text{eff}-C}^{\text{tri}-b})^2}{E} \frac{1 + \sqrt{1 + (4/\pi^2) \sin^4(\pi\phi/2)}}{2}, \tag{25}$$

where $K_{\text{eff}-C}^{\text{tri}-b}$ is the K-based effective fracture toughness for crack tri-branching and can be written as

$$K_{\text{eff}-C}^{\text{tri}-b} = \max\left\{K_{\text{eff}-C}^{A_2\text{-wing}}, K_{\text{eff}-C}^{A_1+A_4\text{-ext}}\right\} = K_{\text{eff}-C}^{A_2\text{-wing}}. \tag{26}$$

The relationship between $G_{\text{max}}^{A_2\text{-wing}}$, $G_{\text{max}}^{A_1+A_4\text{-ext}}$ and $G_{\text{max}}^{\text{tri}-b}$ may be schematically shown in Fig. 9. The K-based criterion for Mode-I/III crack tri-branching can be found as:

$$K_{\text{eff}} = K_{\text{eff}-C}^{\text{tri}-b}. \tag{27}$$

4.3 Another case of mixed Mode-I/III crack tri-branching

Taking some non-idealized crack tips or the other disturbance into consideration, such as a notch tip, a new-born crack should initiate only from the subboundary A_1 or A_4 as a form of extension as shown in Fig. 10. In this case, a potential fracture configuration of crack tri-branching, i.e. three new-born cracks initiation from sub boundaries A_1 , A_2 and A_3 , respectively, should be triggered. Then, another form of mixed Mode-I/III

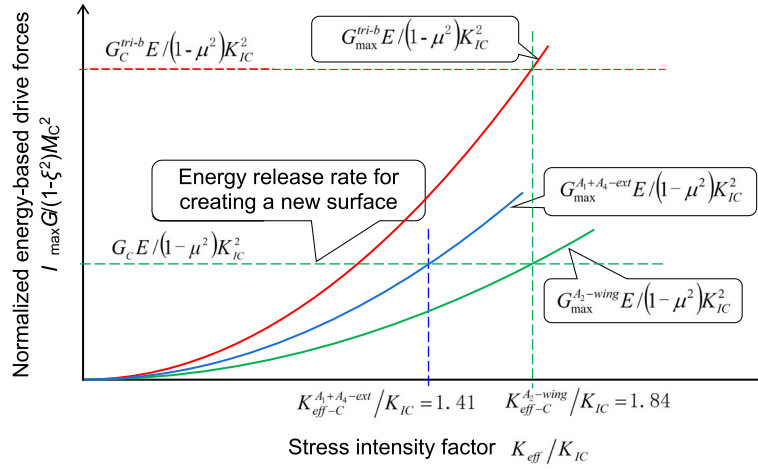


Fig. 9 The relationship between $G_{\max}^{A_2\text{-wing}}$, $G_{\max}^{A_1+A_4\text{-ext}}$ and G_{\max}^{tri-b}

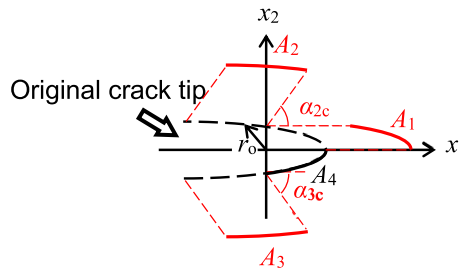


Fig. 10 Another form of Mode-I/III crack tri-branching

crack tri-branching may be formed. By using the same way in Sects. 4.1–4.2, the energy-based configuration driving force for mixed Mode-I/III crack tri-branching can be given by

$$G_{\max}^{tri-b} = \frac{(1 - \mu^2)(K_I^2 + K_{III}^2/(1 - \mu))}{E} \frac{1 + 2\sqrt{1 + (4/\pi^2) \sin^4(\pi\varphi/2)}}{4}. \quad (28)$$

The energy-based driving force for crack initiation from A_1 in a form of crack extension can be found as

$$G_{\max}^{A_1\text{-ext}} = \frac{(1 - \mu^2)(K_I^2 + K_{III}^2/(1 - \mu))}{E} \frac{1}{4}. \quad (29)$$

From Eqs. (19), (20) and (29), the K-based fracture toughness of the local boundary A_1 can be found as.

$$K_{\text{eff-C}}^{A_1\text{-ext}} = 2K_{IC}. \quad (30)$$

Then, from Eqs. (18) and (28), the critical energy release rate for mixed Mode-I/III crack tri-branching can be found as

$$G_C^{tri-b} = \frac{(1 - \mu^2)(K_{\text{eff-C}}^{tri-b})^2}{E} \frac{1 + 2\sqrt{1 + (4/\pi^2) \sin^4(\pi\varphi/2)}}{4}, \quad (31)$$

where the K-based effective fracture toughness can be expressed by

$$K_{\text{eff-C}}^{tri-b} = \max\{K_{\text{eff-C}}^{A_2\text{-wing}}, K_{\text{eff-C}}^{A_1\text{-ext}}\} = K_{\text{eff-C}}^{A_1\text{-ext}} = 2K_{IC}, \quad (32)$$

which is schematically shown in Fig. 8.

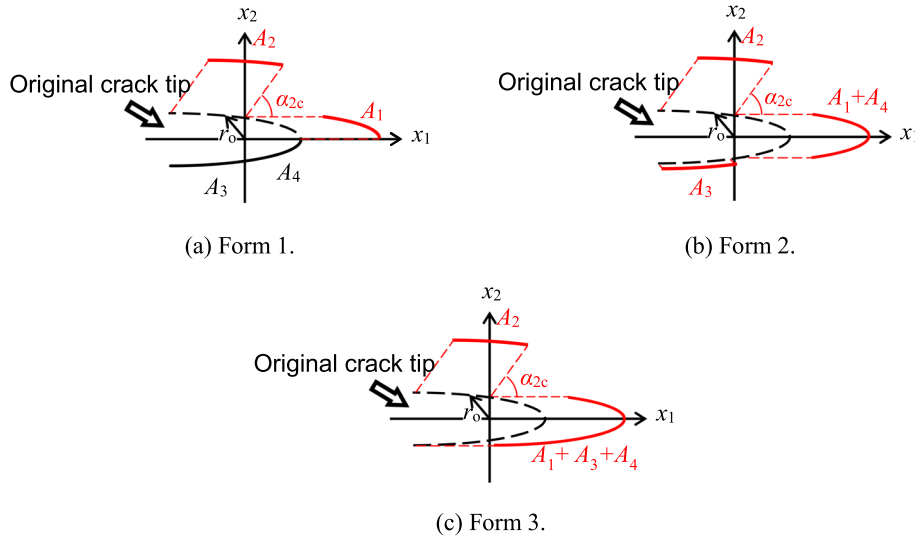


Fig. 11 The geometrical sketch on the three potential forms of mixed Mode-I/III crack side-branching

Table 2 The normalized energy-based configuration driving forces and K-based effective fracture toughness for mixed Mode-I/III crack side-branching

Fracture configuration (Fig. 11)	$EG_{\max}^{\text{side-b}} / (1 - \mu^2) K_{\text{eff}}^2$	$K_{\text{eff-C}}^{\text{side-b}}$
Form 1	$\frac{1 + \sqrt{1 + (4/\pi^2) \sin^4(\pi\varphi/2)}}{4}$	$\max \{ K_{\text{eff-C}}^{A_2\text{-wing}}, K_{\text{eff-C}}^{A_1\text{-ext}} \} = K_{\text{eff-C}}^{A_1\text{-ext}} = 2K_{IC}$
Form 2	$\frac{2 + \sqrt{1 + (4/\pi^2) \sin^4(\pi\varphi/2)}}{4}$	$\max \{ K_{\text{eff-C}}^{A_2\text{-wing}}, K_{\text{eff-C}}^{A_1+A_4\text{-ext}} \} = K_{\text{eff-C}}^{A_2\text{-wing}}$
Form 3	$\frac{3 + \sqrt{1 + (4/\pi^2) \sin^4(\pi\varphi/2)}}{4}$	$\max \{ K_{\text{eff-C}}^{A_2\text{-wing}}, K_{\text{eff-C}}^{A_1+A_3+A_4\text{-ext}} \} = K_{\text{eff-C}}^{A_2\text{-wing}}$

4.4 Mixed Mode-I/III crack side-branching

There are theoretically three forms of potential mixed Mode-I/III crack side-branching as shown in Fig. 11. By using the same way discussed in Sects. 4.1 and 4.2, the energy-based configuration driving forces and K-based effective fracture toughness for mixed Mode-I/III crack side-branching can be found and listed in Table 2.

4.5 Mixed Mode-I/III crack branching and kinking

When two cracks initiate, respectively, from boundaries A_2 and A_3 inward to solids as two wing cracks, the potential and classical crack branching should be formed as shown in Figs. 5b and 12a. In this case, the concerned energy-based configuration driving force can be expressed as

$$G_{\max}^{\text{sym-b}} = \frac{(1 - \mu^2)(K_I^2 + K_{III}^2/(1 - \mu)) \sqrt{1 + (4/\pi^2) \sin^4(\pi\varphi/2)}}{E \cdot 2} \tag{33}$$

The K-based effective fracture toughness for mixed Mode-I/III crack branching can be given by

$$K_{\text{eff-C}}^{\text{sym-b}} = K_{\text{eff-C}}^{A_2\text{-wing}} = \frac{2}{[1 + (4/\pi^2) \sin^4(\pi\varphi/2)]^{1/4}} K_{IC} \tag{34}$$

If only one wing crack initiates from A_2 or A_3 as a form of crack kinking as shown in Fig. 12b, the concerned energy-based configuration driving force becomes

$$G_{\max}^{\text{kinking}} = \frac{(1 - \mu^2)(K_I^2 + K_{III}^2/(1 - \mu)) \sqrt{1 + (4/\pi^2) \sin^4(\pi\varphi/2)}}{E \cdot 4} \tag{35}$$

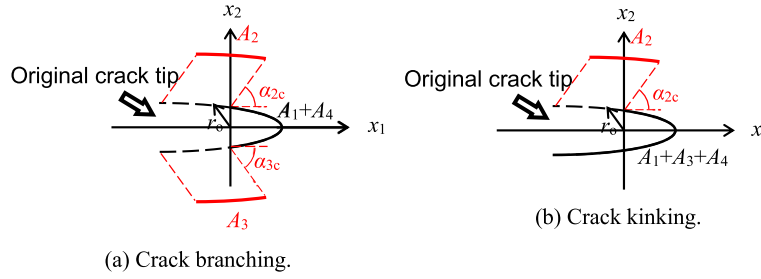


Fig. 12 The geometrical sketch on the enlarged mixed Mode-I/III crack symmetrical branching and kinking

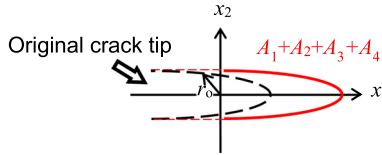


Fig. 13 Crack extension under mixed Mode-I/III loading

The K-based effective fracture toughness for mixed Mode-I/III crack kinking can be given by

$$K_{\text{eff-C}}^{\text{kinking}} = K_{\text{eff-C}}^{A_2\text{-wing}} = \frac{2}{[1 + (4/\pi^2) \sin^4(\pi\varphi/2)]^{1/4}} K_{IC}. \tag{36}$$

4.6 On mixed Mode-I/III crack extension

As shown in Fig. 13, when the moving of the whole boundary $A = A_1 + A_2 + A_3 + A_4$ in x_1 -direction as a form of crack extension is triggered, from Table 1, the corresponding energy-based driving force can be found

$$G_{\text{max}}^{A\text{-ext}} = \frac{(1 - \mu^2)(K_I^2 + K_{III}^2/(1 - \mu))}{E}, \tag{37}$$

which is consistent with the classical J -integral method. Then, from Eqs. (19), (20) and (37), the K-based effective fracture toughness for mixed Mode-I/III crack extension can be given by.

$$K_{\text{eff-IC}}^{A\text{-ext}} = K_{IC}. \tag{38}$$

When the local boundary A_1 , $A_1 + A_4$ (or $A_1 + A_2$) or $A_1 + A_3 + A_4$ moves in x_1 -direction, from Table 1 and Eqs.(19), (20), (22), (24) and (29) and by using the same way, it is not difficult to get the K-based effective fracture toughness

$$K_{\text{eff-IC}}^{A\text{-ext}} = \begin{cases} 2K_{IC}, & A_1 \text{ moving and } A = A_1 \\ \sqrt{2}K_{IC}, & A_1 + A_4 \text{ moving and } A = A_1 + A_4 \text{ or } A_1 + A_2 \\ (2/\sqrt{3})K_{IC}, & A_1 + A_3 + A_4 \text{ moving and } A = A_1 + A_3 + A_4 \end{cases}. \tag{39}$$

Equations (38) and (39) indicate that there are four potential K-based effective fracture toughness for crack straight propagation under mixed Mode-I/III loading, which is similar to the case of the pure Mode-I deformation [28].

5 Triggering for mixed Model-I/III crack multiple-branching

As discussed in the above sections, for a cracked solid under mixed Mode-I/III loading, there are many forms of the potential fracture configurations. Obviously, the real fracture configuration may be one of them, which is triggered under proper conditions. There are many factors that affect the fracture behaviours, including

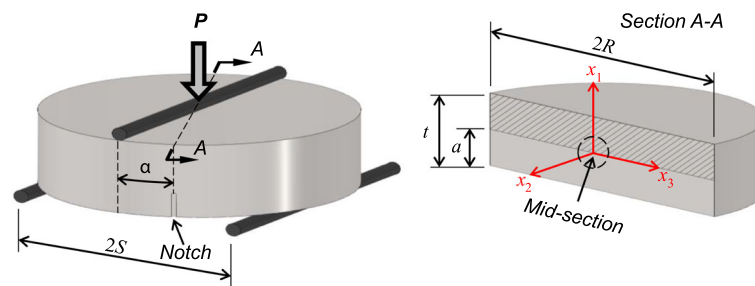


Fig. 14 Geometry and loading sketch of the ENDB specimen

the geometrical shape of the crack/flaw tip [16], the way of loading [15] and the disturbance from a weak Mode-II loading [21], etc. Taking the notch tip for example, if the width of which is narrow enough, the mixed Mode-I/III stress fields are approximately correct and the fracture configurations as shown in Figs. 11a and 12 are most likely to be triggered because A_1 and A_4 cannot move together in x_1 -direction. Moreover, as the difference between the driving forces $G_{\max}^{A_2\text{-wing}}$ and $G_{\max}^{A_1\text{-ext}}$, only wing crack/cracks in form of the crack kinking/branching as shown in Fig. 12 will be triggered under quasi-static mixed Mode-I/III loading. Additionally, if increasing loading rate or even impulse mixed Mode-I/III loading, the $G_{\max}^{A_2\text{-wing}}$ and $G_{\max}^{A_1\text{-ext}}$ may reach the critical values simultaneously or in a enough short time period. Then two cracks, respectively, initiate from the local boundaries A_1 and A_2 . The potential mixed Mode-I/III crack multiple-branching, such as the crack side-branching as shown in Fig. 11a, should be triggered similar to the cases of pure Mode-I [22] and pure Mode-II deformation [23].

The dynamical nature of the crack branching has been one of the focuses in fracture mechanics. Yoffe [29] argued that the maximum $\sigma_{\theta\theta}$ stress acted normal to lines that make an angle of 60° with the direction of crack propagation when the crack velocity exceeded 60% of the shear wave speed. Therefore, she suggested that this fact might cause the crack to branch whenever the crack velocity exceeded that value. Ravi-Chandar and Knauss [30] suggested that crack branching is a natural evolution from a "cloud" of micro-cracks that accompany and lead the main crack. Present analysis, including the works [21–23], provides an alternative energy-based fracture mechanism for crack multiple-branching.

6 Experimental observations on cracked specimen under mixed Mode-I/III loading

A new test configuration called the edge notched disc bend specimen (ENDB) [31–36] had been recently suggested to investigate the fracture behaviour of a cracked solid under mixed Mode-I/III loading as shown in Fig. 14. This disc-shaped specimen with radius R and thickness t is subjected to three-point bend loading. An edge narrow notch of depth a is created through the disc diameter. The crack plane makes an inclination angle of α relative to the loading rollers. The extensive three-dimensional finite element analyses and experimental fracture investigations were performed for different geometrical parameters and loading conditions to introduce full combinations of mixed Mode-I/III ranging from pure Mode-I to pure Mode-III [31–36] by changing the crack inclination angle α . Then, the effectiveness of the ENDB specimen had been verified.

Usually, different K_I , K_{II} and K_{III} values can be expected along the notch tip front as shown in Fig. 14. However, because the x_1 - x_2 plane is an antisymmetric plane of Mode-II deformation, K_{II} tends to zero when $x_3 \rightarrow 0$, which creates a stable condition of mixed Mode-I/III loading around $x_3 = 0$. Numerical results [29] indicated that at the mid-section of the ENDB specimen, the effective stress intensity factor will reach its maximum value and the local notch front around $x_3 = 0$ will fracture first. It should be noted that the fracture configuration at $x_3 = 0$ presents a form of crack extension because of the antisymmetric Mode-II deformation, which is also a typical underlying fracture configuration predicted by present method and is the most energetically favourable in this case. Then the critical load can be used to investigate the fracture behaviours of a cracked solid under mixed Mode-I/III loading [31–36].

In order to get the fracture toughness of PUR foams, a series of experiments had been conducted [32]. Some typical fracture configurations of the tested ENDB polyurethane specimens under different Mode mixities are shown in Fig. 15 [32]. The theoretical normalized effective fracture toughness predicted by present method and experimental values are listed in Table 3 and sketched in Fig. 16, which indicate that the theoretical values are

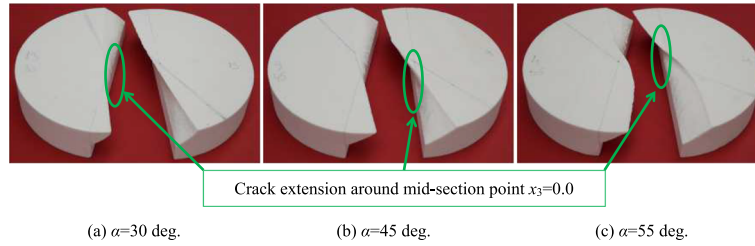


Fig. 15 Typical fracture configurations for polyurethane ENDB specimens under typical Mode mixities [32]

Table 3 The theoretical and experimental normalized effective fracture toughness ($\mu = 0.333$) [32]

Foam density ρ_f (kg/m ³)	α (°)	Avg P_c (N)	K_I (MPa.m ^{0.5})	K_{III} (MPa.m ^{0.5})	K_{eff-C}/K_{eff-IC} (MPa.m ^{0.5})
100	0	177.00	$K_{eff-IC} = 2.89$	0	1.0
	30	230.67	2.33	0.64	1.02
	45	369.00	1.99	1.15	0.97
	55	500.00	1.19	1.49	0.81
	59	579.33	0.27	1.65	0.71
	64	623.33	0	1.75	0.74
145	0	225.00	$K_{eff-IC} = 3.56$	0	1.0
	30	407.67	4.08	1.12	1.46
	45	545.00	2.19	1.68	0.95
	55	615.67	1.46	1.83	0.81
	59	818.00	1.00	2.30	0.86
	64	1063.00	0	2.90	0.997
300	0	529.67	$K_{eff-IC} = 10.87$	0	1.0
	30	788.00	9.99	2.75	1.17
	45	1180.00	8.02	4.63	1.04
	55	1643.33	4.89	6.13	0.88
	59	1713.33	2.64	6.07	0.75
	64	1910.00	0	6.683	0.75

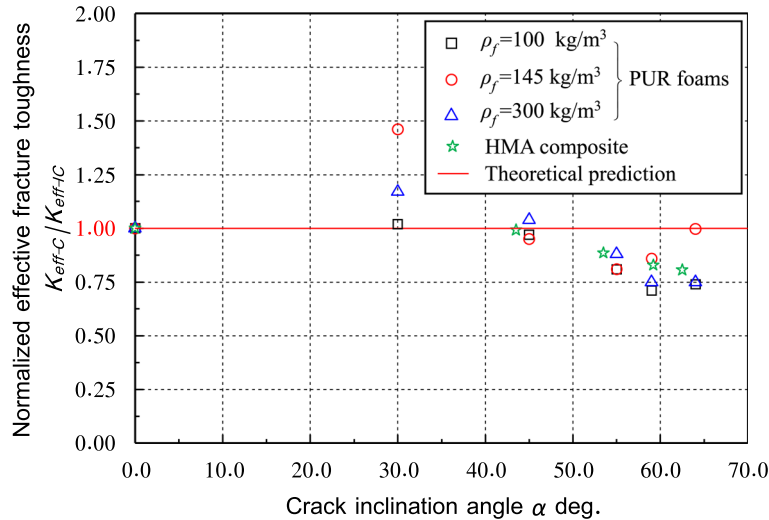


Fig. 16 Theoretical and experimental K-based effective fracture toughness

basically the same with the experimental values. From Fig. 15, it is not difficult to observe that the local fracture configuration of tested polyurethane ENDB specimens at $z = 0$ is obviously the form of crack extension.

Similar fracture configuration had been observed from the ENDB specimens made of hot mix asphalt (HMA) composites [33]. The theoretical and experimental normalized effective fracture toughness values are listed in Table 4 and schematically shown in Fig. 16.

Table 4 The theoretical and experimental normalized effective fracture toughness ($\mu = 0.35$) [33]

Test no	α (°)	P_c (N)	K_I (MPa.m ^{0.5})	Avg K_I (MPa.m ^{0.5})	K_{III} (MPa.m ^{0.5})	Avg K_{III} (MPa.m ^{0.5})	Ave K_{eff-C}/K_{eff-IC} (MPa.m ^{0.5})
1	0	723	0.665	$K_{eff-IC} = 0.686$	0	0	1.0
2		735	0.676		0		
3		754	0.694		0		
4		770	0.709		0		
5	43.5	2155	0.601	0.611	0.239	0.241	0.992
6		2105	0.587		0.233		
7		2198	0.631		0.243		
8		2231	0.623		0.247		
9	53.5	3527	0.366	0.381	0.366	0.381	0.885
10		3625	0.377		0.377		
11		3710	0.385		0.385		
12		3804	0.395		0.395		
13	59.2	4520	0.182	0.174	0.456	0.436	0.828
14		4390	0.177		0.443		
15		4253	0.172		0.429		
16		4125	0.166		0.416		
17	62.5	4435	0	0	0.435	0.446	0.806
18		4314	0		0.423		
19		4603	0		0.452		
20		4812	0		0.472		

7 Conclusions

A three-dimensional modelling has been proposed to formulize the physical process of multiple cracks initiation from a crack tip under mixed Mode-I/III loading. Present analysis indicates that at the onset of fracture, the moving of the new-born cracks remains in the plane perpendicular to x_3 -axis (crack front) because of the $J_3 = 0.0$. Based on the present energy-based modelling, in order to maximize the energy release rate, it is reasonable that the whole boundary around a crack tip should be theoretically divided into four subintervals. Then the four energy-based driving forces can be found, which will drive the four sub boundaries to fracture in form of either wing cracks or extension. The energy-based driving forces have three basic elements, i.e. the point of application, direction and magnitude. So the potential fracture configurations for cracked solids under the mixed Mode-I/III loading, such as the crack tri-branching, symmetrical branching, side-branching, kinking and extension, can be theoretically predicted from the combinations of the new triggered cracks. The present investigations should refresh the understanding on the complex fracture phenomena in the specimen and the engineering structures, such as the hydraulic fracturing for getting more abundant hydraulic crack system.

The physical nature of the experimental fracture phenomenon can be easily recognized based on the present modelling. By comparing the experimental fracture configurations with the potential fracture configurations predicted by present method, which form of the underlying fracture configuration and the fracture mechanism, such as crack side-branching, kinking and extension, can be identified. Then, the corresponding energy-based configuration driving force, K-based effective fracture toughness and fracture criterion can be clearly known. The experimental observations on the ENDB specimens made of PUR foams and HMA composites under mixed Mode-I/III loading indicate that the fracture configuration in form of the crack extension at the mid-section $x_3 = 0$ of the specimen has been verified, which is one of the typical potential fracture configurations predicted by present modelling. The normalized K-based effective fracture toughness predicted in this article agree well with the experimental values.

From the present investigations, there are four potential K-based fracture toughness for crack extension. It is therefore reasonable to speculate that the experimental data should be scattered from an infinitely sharp crack to a blunt notch, which is similar to the additive effect of crack-tip damage zones [37].

Acknowledgements This work was supported by National Natural Science Foundation of China (Grant Nos.: 50771052, 50971068 and 11272141) and Natural Science Foundation of Liaoning (Grant Nos.: LS2010100 and 20102129).

References

1. Aliha, M.R.M., Ayatollahi, M.R.: Analysis of fracture initiation angle in some cracked ceramics using the generalized maximum tangential stress criterion. *Int. J. Solids Struct.* **49**, 1877–1883 (2012)
2. Erdogan, F., Sih, G.C.: On the crack extension in plates under plane loading and transverse shear. *J. Basic Eng. Trans ASME.* **85**, 519–525 (1963)
3. Sih, G.C.: Strain-energy-density factor applied to mixed Mode crack problems. *Int. J. Fract.* **10**, 305–321 (1974)
4. M. A. Hussain, S. L. Pu, J. Underwood.: (1974) Strain energy release rate for a crack under combined Mode I and Mode II. Fracture Analysis., ASTM STP 560. American Society for Testing and Materials, Philadelphia, pp. 2–28.
5. Akbardoost, J., Ayatollahi, M.R., Aliha, M.R.M., Pavier, M.J., Smith, D.J.: Size-dependent fracture behavior of Guiting limestone under mixed Mode loading. *Int. J. Rock Mech. Min. Sci.* **71**, 369–380 (2014)
6. Aliha, M.R.M., Hosseinpour, Gh.R., Ayatollahi, M.R.: Application of cracked triangular specimen subjected to three-point bending for investigating fracture behavior of rock materials. *Rock Mech. Rock Eng.* **46**, 1023–1034 (2013)
7. Mirsayar, M.M., Razmi, A., Aliha, M.R.M., Berto, F.: EMTSN criterion for evaluating mixed mode I/II crack propagation in rock materials. *Eng. Fract. Mech.* **190**, 186–197 (2018)
8. Aliha, M.R.M., Berto, F., Mousavi, A., Razavi, S.M.J.: On the applicability of ASED criterion for predicting mixed mode I+II fracture toughness results of a rock material. *Theor. Appl. Fract. Mech.* **92**, 198–204 (2017)
9. Razavi, S.M.J., Aliha, M.R.M., Berto, F.: Application of an average strain energy density criterion to obtain the mixed mode fracture load of granite rock tested with the cracked asymmetric four-point bend specimens. *Theor. Appl. Fract. Mech.* **97**, 419–425 (2018)
10. Cotterell, B., Rice, J.R.: Slightly curved or kinked cracks. *Int. J. Fract.* **16**, 155–169 (1980)
11. Lin, B., Mear, M.E., Ravi-Chandar, K.: Criterion for initiation of cracks under mixed-mode I+III loading. *Int J Fract.* **165**, 175–188 (2010)
12. Pons, A.J., Karma, A.: Helical crack-front instability in mixed-mode fracture. *Nature* **464**, 85–89 (2010)
13. Chen, C.H., Cambonie, T., Lazarus, V., Nicoli, M., Pons, A.J., Karma, A.: Crack front segmentation and facet coarsening in mixed-mode fracture. *Phys. Rev. Lett.* **115**, 265503 (2015)
14. Pollard, D.D., Segall, P., Delaney, P.T.: Formation and interpretation of dilatant echelon cracks. *Geol. Soc. Am. Bull.* **93**, 1291–1303 (1982)
15. Karma, A., Kessler, D.A., Levine, H.: Phase-field model of mode III dynamic fracture. *Phys. Rev. Lett.* **87**, 045501 (2001)
16. Hakim, V., Karma, A.: Crack path prediction in anisotropic brittle materials. *Phys. Rev. Lett.* **95**, 235501 (2005)
17. Hakim, V., Karma, A.: Laws of crack motion and phase-field models of fracture. *J. Mech. Phys. Solids* **57**, 342–368 (2009)
18. Meggiolaro, M.A., Miranda, A.C.O.: Stress intensity factor equations for branched crack growth. *Eng. Fract. Mech.* **72**, 2647–2671 (2005)
19. Li, X.H., Zheng, X.Y., Yuan, W.J., Cui, X.W., Xie, Y.J., Wang, Y.: Instability of cracks initiation from a mixed-mode crack tip with iso-stress intensity factors KI and KII. *Theor. Appl. Fract. Mech.* **96**, 262–271 (2018)
20. Xie, Y.J., Li, J., Hu, X.Z., Wang, X.H., Cai, Y.M., Wang, W.: Modelling of multiple crack-branching from Mode-I crack-tip in isotropic solids. *Eng. Fract. Mech.* **109**, 105–116 (2013)
21. Xie, Y.J., Duo, Y.L., Yuan, H.: Potential fracture paths for cracked rocks under compressive-shear loading. *Int. J. Rock Mech. Min. Sci.* **128**, 104216 (2020)
22. Yuan, H., Xie, Y.J., Wang, W.: Underlying fracture trends on mode-I crack multiple-branching. *Eng. Fract. Mech.* **225**, 106835 (2020)
23. Li, J., Xie, Y.J., Zheng, X.Y., Cai, Y.M.: Underlying fracture trends and triggering on Mode-II crack branching and kinking for quasi-brittle solids. *Eng. Fract. Mech.* **211**, 382–400 (2019)
24. Eshelby, J.D.: The force on an elastic singularity. *Phil Trans. Roy. Soc. London Ser A.* **244**, 87–112 (1951)
25. Budiansky, B., Rice, J.R.: Conservation laws and energy-release rates. *ASME J. Appl. Mech.* **40**, 201–203 (1973)
26. Griffith, A.A.: The phenomena of rupture and flow in solids. *Phil. Trans. Roy. Soc. Lon. Ser. A.* **221**, 163–198 (1921)
27. Cherepanov, G.P.: Mechanics of brittle fracture, Moscow, Publish House “Nuaka”, 1974, pp. 266–269. English translation published by McGraw-Hill International Book Co., New York (1979)
28. Yuan, H., Xie, Y.J.: Disturbance effects of weak Mode-II loading on K-based Mode-I fracture toughness test. *Theor. Appl. Fract. Mech.* **110**, 102822 (2020)
29. Yoffe, E.: The moving griffith crack. *Phil. Mag.* **42**, 739–750 (1951)
30. Ravi-Chandar, K., Knauss, W.G.: An experimental investigation into dynamic fracture: III. On steady-state crack propagation and crack branching. *Int. J. Fract.* **26**, 141–154 (1984)
31. Aliha, M.R.M., Bahmani, A., Akhondi, Sh.: Numerical analysis of a new mixed mode I/III fracture test Specimen. *Eng. Fract. Mech.* **134**, 95–110 (2015)
32. Aliha, M.R.M., Linul, E., Bahmani, A., Marsavina, L.: Experimental and theoretical fracture toughness investigation of PUR foams under mixed mode I+III loading. *Polym. Testing* **67**, 75–83 (2018)
33. Aliha, M.R.M., Bahmani, A., Akhondi, Sh.: A novel test specimen for investigating the mixed mode I + III fracture toughness of hot mix asphalt composites—experimental and theoretical study. *Int. J. Solids Struct.* **90**, 167–177 (2016)
34. Aliha, M.R.M., Berto, F., Bahani, A., Akhondi, Sh., Barnoush, A.: Fracture assessment of polymethyl methacrylate using sharp notched disc bend specimens under mixed mode I+III loading. *Phys. Mesomech.* **19**, 355–364 (2016)
35. Aliha, M.R.M., Bahmani, A., Akhondi, Sh.: Determination of mode III fracture toughness for different materials using a new designed test configuration. *Mater. Des.* **86**, 863–871 (2015)
36. Aliha, M.R.M., Bahmani, A.: Rock fracture toughness study under mixed mode I/III loading. *Rock Mech. Rock Eng.* **50**, 1739–1751 (2017)
37. Hu, X.: Additive effect of micro-damage zones from nano-scale crack tip and nano-grains for fracture toughness measurements of 3Y-TZP zirconia. *J. Eur. Ceram. Soc.* **42**(15), 7174–7179 (2022)

Publisher's Note Springer Nature remains neutral with regard to jurisdictional claims in published maps and institutional affiliations.

Springer Nature or its licensor (e.g. a society or other partner) holds exclusive rights to this article under a publishing agreement with the author(s) or other rightsholder(s); author self-archiving of the accepted manuscript version of this article is solely governed by the terms of such publishing agreement and applicable law.